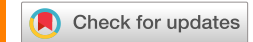
RESEARCH ARTICLE | SEPTEMBER 16 2024

## Floating-point photonic iterative solver demonstrated for Newton–Raphson method $\odot$

Andrew B. Klein ■ (i); Zheyuan Zhu (ii); Guifang Li (iii); Shuo Pang (iii)



Appl. Phys. Lett. 125, 121108 (2024) https://doi.org/10.1063/5.0216999









# Floating-point photonic iterative solver demonstrated for Newton-Raphson method

Cite as: Appl. Phys. Lett. **125**, 121108 (2024); doi: 10.1063/5.0216999 Submitted: 2 May 2024 · Accepted: 1 September 2024 · Published Online: 16 September 2024







Andrew B. Klein, <sup>a</sup> 🕞 Zheyuan Zhu, 🕞 Guifang Li, 🕞 and Shuo Pang 🕞

#### **AFFILIATIONS**

CREOL, The College of Optics and Photonics at the University of Central Florida, Orlando, Florida 32816, USA

a) Author to whom correspondence should be addressed: Andrew. Klein@ucf.edu

#### **ABSTRACT**

Though photonic computing systems offer advantages in speed, scalability, and power consumption, they often have a limited dynamic encoding range due to low signal-to-noise ratios. Compared to digital floating-point encoding, photonic fixed-point encoding limits the precision of photonic computing when applied to scientific problems. In the case of iterative algorithms such as those commonly applied in machine learning or differential equation solvers, techniques like precision decomposition and residue iteration can be applied to increase accuracy at a greater computing cost. However, the analog nature of photonic symbols allows for modulation of both amplitude and frequency, opening the possibility of encoding both the significand and exponent of floating-point values on photonic computing systems to expand the dynamic range without expending additional energy. With appropriate schema, element-wise floating-point multiplication can be performed intrinsically through the interference of light. Herein, we present a method for configurable, signed, floating-point encoding and multiplication on a limited precision photonic primitive consisting of a directly modulated Mach–Zehnder interferometer. We demonstrate this method using Newton's method to find the Golden Ratio within ±0.11%, with six-level exponent encoding for a signed trinary digit-equivalent significand, corresponding to an effective increase of 243× in the photonic primitive's dynamic range.

Published under an exclusive license by AIP Publishing. https://doi.org/10.1063/5.0216999

While CPUs and digital accelerators such as GPUs store numbers in floating-point (FLP) format to guarantee high-precision operations, photonic or analog computing uses signal amplitude equivalent to fixed-point (FXP) format, which accommodates limited signal-tonoise ratio (SNR) and reduces data storage requirements. The adoption of FXP encoding guarantees an inherent error for any computing applications, and while in some cases this is not detrimental, it often leads to errors in iterative or high-precision solutions. For example, our previous work on creating a photonic eigensolver showed that using signed 4-bit FXP precision is not sufficient to achieve FLPequivalent accuracy. Techniques such as precision decomposition<sup>2</sup> and residue iteration<sup>3</sup> can be used to increase the accuracy, but they often involve exponentially increased computation requirements and slower rates of convergence. Ultimately, for use in scientific computing, optics must provide not only scalability and energy efficiency but also precision.

In digital floating-point (D-FLP) encoding, each value A is broken down into a significand  $s_A$  and corresponding exponent  $l_A$  with a global base  $\beta$  such that  $A = s_A \times \beta^{l_A}$ . For the 32-bit D-FLP encoding, the significand and exponent are recorded within 31 bits using a global base of 2 or 10. To multiply two numbers, their significands undergo

bitwise multiplication, their exponents are added, and an XOR operation is performed on the sign bits of each significand,<sup>5</sup> such that  $A \times B = (s_A \times \beta^{l_A}) \times (s_B \times \beta^{l_B}) = s_A s_B \times \beta^{l_A + l_B}$ . Each process requires energy for computation. Previous attempts to unionize D-FLP encoding and optical/photonic multipliers have tried to replicate the bitwise operations on binarized optically encoded vectors. 6 However, individually encoding each bit with only "0" and "1" states is untenable for an optical system, as encoding 32- or 64-bit floating-point values would require too large a format to scale to the millions of computations required for modern computing applications. Additionally, optical amplitude modulation can accommodate an integer base  $\beta$ , which is greater than 2; methods such as pulse or quadrature amplitude modulation (PAM or QAM) can produce between 4 and 64 levels as long as the signal-to-noise ratio (SNR) allows.<sup>7-9</sup> Therefore, a nonbinarized optical multiplicand could be represented with fewer "optical bits" than the binary D-FLP representation.

This work demonstrates photonic floating-point encoding (P-FLP), a method for implementing FLP encoding on photonic computing architectures using amplitude and frequency to represent significand and exponent, respectively. P-FLP encoding enables passive significand multiplication and exponent addition operations to

increase energy efficiency and expand the dynamic range of photonic computing systems. Utilizing (P-FLP) encoding, a photonic multiplication primitive with five signed input levels was used to implement the Newton–Raphson root finding algorithm to find the Golden Ratio. The P-FLP primitive shows improved accuracy compared to FXP encoding, while maintaining the quadratic convergence rate achievable with D-FLP encoding.

For a coherent optical source with narrow spectrum centered at  $f_0$  modulated by an RF carrier function g(t), the resulting electric field is  $E(t) = g(t) \exp(i2\pi f_0 t)$ . In P-FLP encoding, each multiplicand is encoded as a sub-carrier with amplitude corresponding to the signed significand s and modulation frequency  $f_l$  corresponding to the exponent l, such that  $g(t) \rightarrow g(s, f_l, t)$ . With L available exponents, the dynamic range will increase by a factor of  $\beta^{L-1}$ , corresponding to  $(L-1)\log_2 \beta$  bits.

Multiple methods of performing an element-wise multiplication between two optically encoded vectors have been proposed, including free space <sup>10</sup> and Mach–Zehnder interferometry. <sup>11</sup> Our proposed schema involves use of single-sideband (SSB) modulation <sup>12</sup> using optical frequencies with spacing  $\Delta f$  and selecting the spectral lines representing the FLP exponent to encode P-FLP symbols. In this schema,  $g(s, f_l, t) = s(t) \exp(\pm i 2\pi f_l t)$ , where  $f_l = l \Delta f$ , and the sign of the complex exponent is positive for upper sideband (USB) modulation and negative for lower sideband (LSB) modulation. With the A multiplicand undergoing USB modulation and the B multiplicand undergoing LSB modulation, the resulting electric fields are

$$E_A(s_A, f_{l_A}, t) = s_A(t) \exp(i2\pi f_{l_A} t) \exp(i2\pi f_0 t),$$
 (1a)

$$E_B(s_B, f_{l_R}, t) = s_B(t) \exp(-i2\pi f_{l_R} t) \exp(i2\pi f_0 t).$$
 (1b)

Through coherent mixing, the product of two multiplicands A and B can be determined from the following:<sup>13</sup>

$$I(t) \propto \operatorname{Re}\left\{E_A^* E_B\right\}$$

$$= \operatorname{Re}\left\{s_A(t) \exp(-i2\pi f_{l_A} t) \exp(-i2\pi f_0 t)\right\}$$

$$* s_B(t) \exp(-i2\pi f_{l_B} t) \exp(i2\pi f_0 t)\}$$

$$= \operatorname{Re}\left\{s_A(t) s_B(t)\right\} \cos(2\pi (f_{l_A} + f_{l_B}) t). \tag{2}$$

This implementation eliminates the common carrier frequency  $f_0$ , performing passive exponent addition via sum-frequency generation corresponding to the summed exponents in the result and passive significand multiplication through the interference of light. The significand and exponent can be retrieved through RF signal measurement (e.g., microwave filter banks).

Here, we demonstrate the P-FLP multiplication using direct modulation with RF sub-carrier frequencies to encode the exponents. The photonic primitive depicted in Fig. 1 and used herein consists of a balanced coherent interferometer with independently modulated inputs A and B generating the respective time-division multiplexed (TDM) fields  $E_A$  and  $E_B$ . The resulting inputs undergo balanced photodetection to produce outputs proportional to signed magnitude  $E_A^*E_B$ . The E field amplitude accommodates five signed input levels ( $\pm 2$ ,  $\pm 1$ , and 0). This is the total number of levels for FXP encoding, while FLP encoding increases the effective bitwidth of the system without increasing the signal power or SNR. The sub-carrier modulated symbol is synthesized through a field programmable gate array (FPGA, Xilinx

XCZU49DR) with two input modulators (JDSU IOA-MOD9140) and can reliably accommodate carrier frequencies up to 500 MHz, while the output is digitized by a streaming digitizer sampling at 6.25 GSa/s. Each FLP symbol is repeated for a duration of 200 ns; a symbol duration of sub 10 ns can be used in theory. For this schema,  $g(s, f_l, t) = s \cdot \cos(2\pi f_l t)$ , and the resulting intensity at the output is proportional to  $s_A s_B \cos(2\pi f_{l_A} t) \cos(2\pi f_{l_B} t)$ .

A sample of the digitized TDM output is shown in Fig. 2(a). To make symbol parsing more reliable, a signed header is added to each packet for parity check. Additionally, a tail of constant positive amplitude is added to verify constructive interference. The output has primary frequency components of  $\pm (f_{l_A} \pm f_{l_B})$ , illustrated in Fig. 2(b). To parse the result, the spectrum is determined by a type-II discrete cosine transform (DCT-II), which intrinsically eliminates any negative frequencies. This leaves frequency components  $f_{l_A} \pm f_{l_B}$ . Since  $f_{l_A} - f_{l_B} < \max(f_{l_A}, f_{l_B}) < f_{l_A} + f_{l_B}$ , manual filtering of any frequencies less than  $\max(f_{l_A}, f_{l_B})$  ensures the dominant remaining frequency will be  $f_{l_A} + f_{l_B}$ , which can be parsed as the exponent of the result. The sign and significand can be determined from the amplitude of the detected signal.

In our previous work, we have demonstrated photonic solvers achieving precision beyond native analog precision by adjusting the exponent of iterative solvers.<sup>2,14</sup> With a floating-point multiplier, we can iteratively solve equations without additional exponent adjustment steps. P-FLP multiplication is especially well-suited for convergent iterative algorithms requiring greater precision, such as root-finding. Here, we use the Newton-Raphson method<sup>15</sup> to demonstrate solving a quadratic equation using P-FLP multiplication. When deployed in floating point, the solution will display a quadratic or better convergence. 16 In order to be deployed on the P-FLP photonic primitive, the function f(x) must be precalculated and stored as a quantized version  $f_q(x)$  using the significands and exponents available to the P-FLP encoding. The inverse derivative D(x) = 1/f'(x) must be similarly precalculated and quantized. With these modifications to accommodate deployment on the photonic primitive of Fig. 1, the Newton-Raphson method takes the form of Algorithm 1, in which  $\times$  denotes P-FLP multiplication.

The modified Newton–Raphson method is well-suited to find roots of quadratic equations so long as the root is not also the vertex. The application demonstrated herein is to find the Golden Ratio  $\varphi$ , defined as the value  $\varphi$  such that  $\varphi = \frac{a}{b} = \frac{a+b}{a}$ , which can be converted to the quadratic equation  $\varphi^2 - \varphi - 1 = 0$ .  $\varphi$  has an accepted value of  $\frac{1+\sqrt{5}}{2} \sim 1.6180$ .

Algorithm 1 was used to solve the Golden Ratio quadratic equation  $f(\varphi) = \varphi^2 - \varphi - 1 = 0$  using P-FLP multiplication over 15 iterations with an initial guess of  $x_0 = 1.2$  [Fig. 3(a)]. The set of exponents corresponding to the distinct carrier frequencies were chosen as  $\{-4, 1\}$ , with global base  $\beta_{FLP} = 3$  to match the signed 5-level

#### ALGORITHM 1. Modified Newton-Raphson method.

```
f_q(x) \leftarrow quantize(f(x)); D_q(x) \leftarrow quantize(D(x));

x_0 \leftarrow Intial\ Guess

for k in range(N):

x_k \leftarrow x_{k-1} - f_q(x_{k-1}) \times D_q(x_{k-1})
```

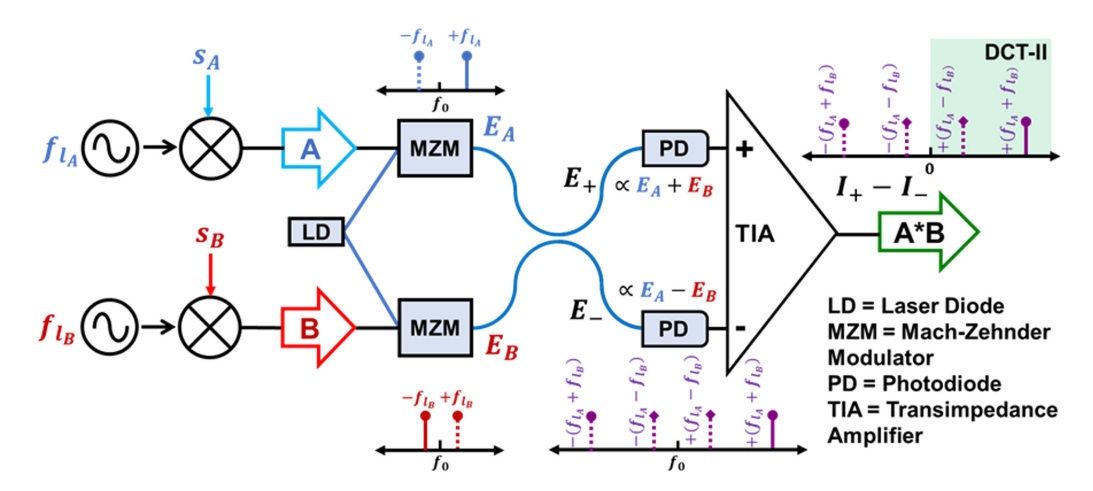


FIG. 1. Schematic for P-FLP multiplication, including representative decomposed frequency components of interim and final results.

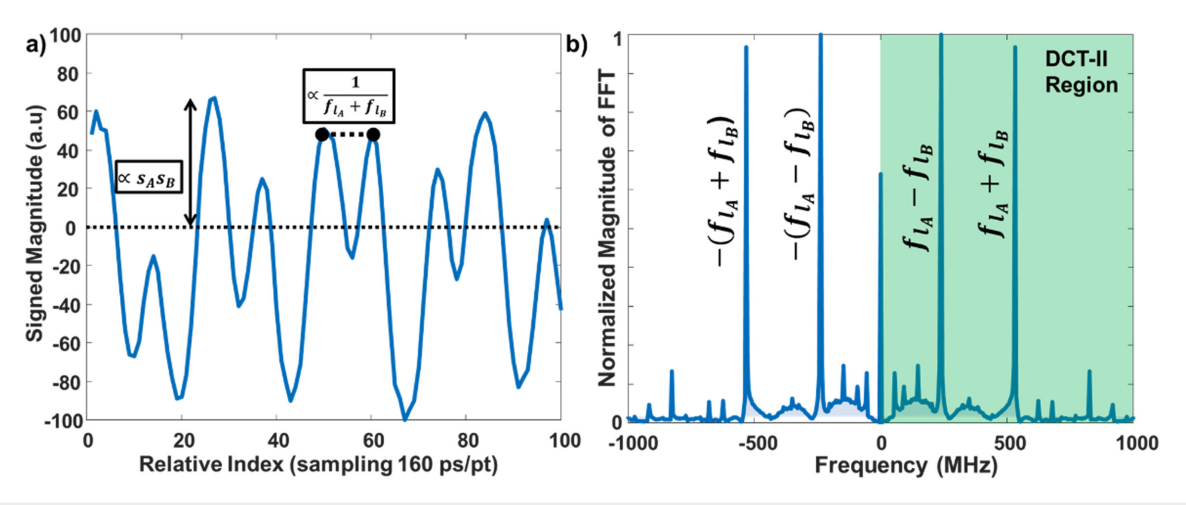


FIG. 2. (a) Sampled experimental waveform output. (b) Experimental spectrum of the digitized output from P-FLP multiplication.

inputs of the photonic primitive. This result was compared to the double-precision D-FLP multiplication as well as base-2 FXP calculation simulated with 129 signed input levels, corresponding to 7-bit fixed point photonic computing systems. f(x) and D(x) were precalculated in the domain [0,4] to minimize quantization error due to the exponent choice. For P-FLP quantization, each value in the precalculated f(x) and D(x) was rounded to its nearest value in the P-FLP encoding schema. For FXP quantization, each value in f(x) and D(x) was encoded as in Eq. (3), corresponding to a global base  $\beta_{FXP}=2$ , and where N is the number of positive FXP levels,

$$f_{q}(x_{i}) = \operatorname{round}\left(\frac{Nf(x_{i})}{2^{\operatorname{floor}(\log_{2}(\max(|f(x)|)))}}\right) \times 2^{\operatorname{floor}(\log_{2}(\max(|f(x)|))) - \operatorname{round}(\log_{2}(N))}.$$
(3)

Figure 3(a) plots the solution path of the modified Newton-Raphson method for solving the Golden Ratio quadratic equation. The

P-FLP implementation converges to  $\varphi=1.6198$ , a result within 0.11% of the accepted value. Compared to the 0.05% error of the double-precision D-FLP on CPU and the 0.24% error of the 129-level FXP implementation, P-FLP offers a significant advantage for limited S/N encoding and approaches the accuracy required for scientific computing. As the model converges closely to the expected value, the number of available FXP levels must be dramatically increased to match the accuracy of the P-FLP implementation. Figure 3(b1) shows that P-FLP and D-FLP maintain quadratic convergence, while the 129-level FXP could not iterate at all with an initial guess of  $x_0=1.6$ , demonstrating that P-FLP encoding offers immediate advantages for photonic computing in expanding the accuracy and effective bitwidth with native photonic SNR.

The P-FLP encoding system predicts an increase in the dynamic range of  $3^5 = 243 \times$ , corresponding to an equivalent of 1215 signed FXP levels (>10 signed bits) in the low-precision photonic primitive. Figure 3(b2) shows that 2049 signed FXP levels (11 signed bits) must be used to exceed the accuracy of the P-FLP implementation, while

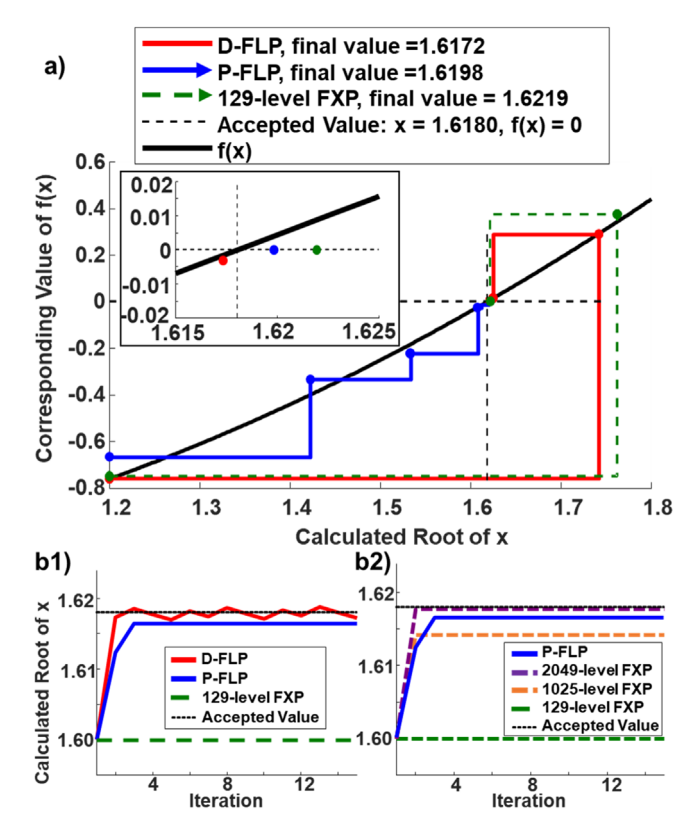
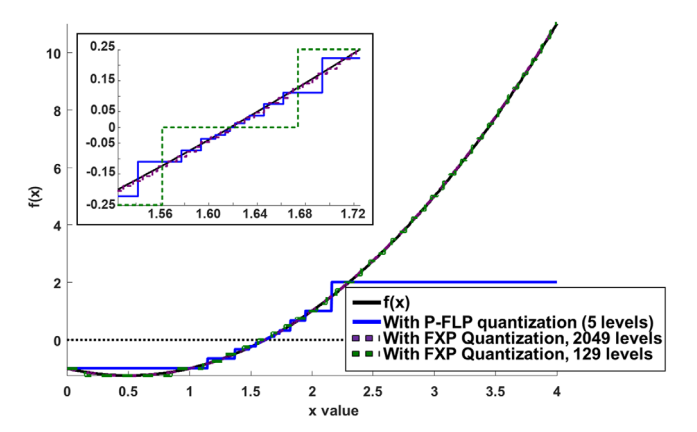


**FIG. 3.** Golden Ratio calculation. (a) Solution path, initial guess  $x_0 = 1.2$ . Inlay shows zoomed convergence locations near the zero. Plotted points indicate final iteration values. (b1) Solution progression by iteration, initial guess  $x_0 = 1.6$ . (b2) Comparison of solution progression.

1025 signed FXP levels (10 signed bits) is not sufficient. For simulations of a further 1500 experiments using random initial guesses of  $x_0$ in the range [1, 2], 5-level P-FLP encoding always converged within 0.2% of the accepted value, while 1025-level FXP encoding only converged to the same accuracy in 92.5% of the results. Thus, the effective increase in the system's dynamic range matches or exceeds predictions. It is reasonable to anticipate that with a better S/N ratio and enough bands to accommodate more than six exponents, the P-FLP implementation could soon match or exceed the performance of the D-FLP implementation. For example, further simulation of 1500 experiments (random initial guesses of  $x_0$  in the range [1, 2]) with expanded P-FLP encoding using six exponents and a signed 257-level significand showed that both P-FLP and D-FLP converge to high accuracy within the same number of iterations; the expanded P-FLP encoding required an average 2.084 iterations (standard deviation, 0.656) to converge within 0.2% of the accepted value, comparable to D-FLP encoding, which required 2.081 iterations (standard deviation, 0.657)

The P-FLP method shows closer convergence than the expanded FXP implementation for two reasons: first, the calculation of  $(f_q(x_{k-1}) \times D_q(x_{k-1}))$  is more accurate, which reduces the chance of overshooting the accepted value and causing the algorithm to find another local minimum or require more iterations for convergence;



 ${f FIG.}$  4. Quantization of f(x) using differing schema. Inlay shows zoomed region of interest near the function root.

second, in the specific case of finding zeros, P-FLP has a smaller minimum encodable value  $q_{\min}$ , which means that the precalculated  $f_q(x)$  has more values encoded closer to the zero. Once  $f_q(x)=0$ , the iteration stops, so the maximum error in a converged result is proportional to  $\frac{q_{\min}}{2}$ . The quantization of  $f_q(x)$  is shown in Fig. 4 for the implemented and simulated schema. For the root-finding application, the chosen exponents for the P-FLP implementation have been optimized to produce better results closer to the root of the equation, at the expense of quantization errors across the remaining domain.

For P-FLP encoding,  $\frac{q_{\min}}{2} = \frac{1 \times \beta^{f_{\min}(l)}}{2} = \frac{1 \times 3^{-4}}{2} \approx 0.006$ , which is consistent with the observed results. For FXP encoding,  $\frac{q_{\min}}{2} = \frac{maximum\ encoded\ value}{2N} = \frac{16}{2N} = \frac{8}{N}$ . With 129 signed levels, N = 64, and the maximum error is  $\pm 0.125$ , so the iteration cannot occur with a close initial guess of  $x_0 = 1.6$ . Once N = 1024,  $\frac{q_{\min}}{2N} \approx 0.008$ , and the FXP implementation can exceed the P-FLP implementation. However, it should be noted that any S/N improvements, which would allow more signed levels in photonic FXP implementations, can immediately be adapted to the P-FLP methodology, further increasing its advantage.

In addition to the predicted increase in the dynamic range, the multiplication, sign operation, and exponent addition are all performed solely through interference; energy is only expended for signal modulation and detection, offering a direct advantage over semiconductor D-FLP systems. These advantages are also scalable; using a frequency comb for the source would allow  $10^2$  frequencies to be used for exponent encoding, with micro-ring resonators used to efficiently select the encoding frequency.

In the current directly modulated implementation, only one operation is carried out using P-FLP multiplication. With further adaptations to the scalable architecture, a majority of mathematical operations can be carried out using P-FLP multiplication. The ideal schema with SSB modulation can be expanded to produce a floating-point photonic matrix-vector multiplier (MVM): For a  $M \times N$  matrix W multiplied by vector X with N elements, each element-wise product  $\mathbf{W}(m,n)\mathbf{X}(n)$  could be encoded in its own modulation arm, then combined together row-wise using an optical multiplexer such that the result  $\mathbf{Y}(m) = \sum_{1}^{N} \mathbf{W}(m,n)\mathbf{X}(n)$ . Using a microwave photonic filter, the accumulated significands and associated exponents for  $\mathbf{Y}(m)$  could

be determined in a single clock cycle. This opens the possibility of photonic inverse solvers, partial differential equation solvers, convolution, and photonic linear layers for neural network applications. <sup>14</sup> Future efforts will be directed to full-scale on-chip deployment of a floating-point photonic tensor accelerator; many of the required elements, including frequency comb sources, <sup>17</sup> MRR frequency selection, <sup>18</sup> and modulation using MZM<sup>19</sup> or MRR, <sup>20</sup> have already been demonstrated on-chip with small formats and reduced power consumption. Additionally, we can apply block decomposition techniques previously demonstrated for our FXP hardware accelerator<sup>2</sup> to further aid scalability.

In summary, we have demonstrated a method for implementing FLP multiplications in photonic computing using the properties of the analog signal to perform sign operations, significand multiplication, and exponent addition without expending energy. Using Newton's method to find the Golden Ratio, P-FLP multiplications produced an accuracy of  $\pm 0.11\%$ , which exceeded the accuracy of 1025-level FXP multiplications. This effectively increased the bitwidth of the system by 243× or more without increased requirements for SNR.

This work was supported in part by the National Science Foundation (No. 1932858), the Army Research Office (No. W911NF2110321), and the Office of Naval Research (No. N00014-20-1-2441).

### AUTHOR DECLARATIONS Conflict of Interest

The authors have no conflicts to disclose.

#### **Author Contributions**

Andrew B. Klein: Conceptualization (equal); Methodology (equal); Software (lead); Writing – original draft (lead); Writing – review & editing (equal). Zheyuan Zhu: Conceptualization (equal); Methodology (equal); Software (supporting); Writing – review & editing (equal). Guifang Li: Conceptualization (equal); Validation (equal); Writing – review & editing (equal). Shuo Pang: Conceptualization (equal); Validation (equal); Writing – review & editing (equal).

#### DATA AVAILABILITY

The data that support the findings of this study are available from the corresponding author upon reasonable request.

#### **REFERENCES**

- <sup>1</sup>A. B. Klein, Z. Zhu, D. Saiham, G. Li, and S. S. Pang, "Iterative eigensolver using fixed-point photonic primitive," Opt. Lett. **49**(2), 194 (2024).
- <sup>2</sup>Z. Zhu, A. B. Klein, G. Li, and S. Pang, "Fixed-point iterative linear inverse solver with extended precision," Sci. Rep. 13(1), 5198 (2023).
- <sup>3</sup>L. F. Richardson, "IX. The approximate arithmetical solution by finite differences of physical problems involving differential equations, with an application to the stresses in a masonry dam," Philos. Trans. R. Soc. London, Ser. A 210(459–470), 307–357 (1911).
- <sup>4</sup>IEEE, "IEEE Standard for Floating-Point Arithmetic," IEEE Std 754-2019 (Revision of IEEE 754-2008) (IEEE, 2019), pp. 1–84.
- <sup>5</sup>M. Rafiquzzaman, Fundamentals of Digital Logic and Microcomputer Design, 5th ed. (Wiley, Germany, 2005).
- <sup>6</sup>R. P. Bocker and W. J. Miceli, US Patent 4,692,885 (8 September 1987).
- <sup>7</sup>L. Zhao, K. Wang, and W. Zhou, "Transmission of 4096-QAM OFDM at D-band," Opt. Express 31(2), 2270 (2023).
- <sup>8</sup>E. El-Fiky, M. Chagnon, M. Sowailem, A. Samani, M. Morsy-Osman, and D. V. Plant, "168-Gb/s single carrier PAM4 transmission for intra-data center optical interconnects," IEEE Photonics Technol. Lett. **29**(3), 314–317 (2017).
- <sup>9</sup>K. Toyoda, Y. Koizumi, T. Omiya, M. Yoshida, T. Hirooka, and M. Nakazawa, "Marked performance improvement of 256 QAM transmission using a digital back-propagation method," Opt. Express 20(18), 19815 (2012).
- <sup>10</sup>J. Spall, X. Guo, T. D. Barrett, and A. I. Lvovsky, "Fully reconfigurable coherent optical vector—matrix multiplication," Opt. Lett. 45(20), 5752 (2020).
- <sup>11</sup>J. Cheng, H. Zhou, and J. Dong, "Photonic matrix computing: From fundamentals to applications," Nanomaterials 11(7), 1683 (2021).
- <sup>12</sup>X. Xu, J. Wu, M. Tan, T. G. Nguyen, S. T. Chu, B. E. Little, R. Morandotti, A. Mitchell, and D. J. Moss, "Photonic single sideband RF generator based on an integrated optical micro-ring resonator," arXiv:1808.08828 (2018).
- <sup>13</sup>K. Kikuchi, "Fundamentals of coherent optical fiber communications," J. Lightwave Technol. 34(1), 157–179 (2016).
- <sup>14</sup>Z. Zhu, A. Fardoost, F. G. Vanani, A. B. Klein, G. Li, and S. S. Pang, "Coherent general-purpose photonic matrix processor," ACS Photonics 11(3), 1189–1196 (2024).
- 15K. Atkinson, An Introduction to Numerical Analysis, 2nd ed. (John Wiley & Sons, Inc., 1991).
- <sup>16</sup>W. C. Campbell, "Convergence of Newton's method for a single real equation," NASA Technical Paper 2489 (NASA, 1985).
- <sup>17</sup>M. Zhang, B. Buscaino, C. Wang, A. Shams-Ansari, C. Reimer, R. Zhu, J. M. Kahn, and M. Lončar, "Broadband electro-optic frequency comb generation in a lithium niobate microring resonator," Nature 568(7752), 373–377 (2019).
- <sup>18</sup>C. Prayoonyong and B. Corcoran, "Optimising microring resonator based optical frequency comb distillation for optical communications systems," Opt. Express 30(11), 17836 (2022).
- <sup>19</sup>B. Desiatov, A. Shams-Ansari, M. Zhang, C. Wang, and M. Lončar, "Ultra-low-loss integrated visible photonics using thin-film lithium niobate," Optica 6(3), 380 (2019).
- <sup>20</sup>Y. Tan, S. Niu, M. Billet, N. Singh, M. Niels, T. Vanackere, J. Van Kerrebrouck, G. Roelkens, B. Kuyken, and D. Van Thourhout, "Micro-transfer printed thin film lithium niobate (TFLN)-on-silicon ring modulator," ACS Photonics 11(5), 1920–1927 (2024).